Validation of a Multi-Grid WAVEWATCH III^{TM}Modeling System*

Arun Chawla[†,1], Hendrik L. Tolman[2], Jeffrey L. Hanson[3], Eve-Marie Devaliere[4], Vera M. Gerald[2]
[1]Science Application International Corporation at NOAA/NCEP
[2]NOAA/NCEP Environmental Modeling Center, Camp Springs MD
[3]USACE Field Research Facility, Duck NC
[4]University of North Carolina/USACE Field Research Facility, Duck NC

1 INTRODUCTION

WAVEWATCH III^{TM}(Tolman, 2002b, 2008), a third generation wind wave spectral model, is the operational wave forecasting model at the National Centers for Environmental Prediction (NCEP). The numerical engine of the model was recently upgraded so that it could be run as a mosaic of grids with two-way exchange of information between overlapping grids (Tolman, 2008). The multi-grid WAVEWATCH III^{TM}was used to develop a new forecast model for NCEP (Chawla et al., 2007) and has been the operational forecast guidance model since December 2007, replacing the older suites of global and nested regional models. The forecast model is driven by the Global Forecast System (GFS - Moorthi et al. 2001).

The modeling system (hereafter referred to as **NMWW3**) consists of 8 grids (see section 2) and has also been used to develop a multi-year global hindcast database that extends from February 2005 to the present. The hindcast runs are generated using the archived analysis winds from GFS. In this paper we shall present a validation study of this system using altimeter data, comparison of bulk statistical properties from a global network of buoys as well as spectral analysis from a subset of buoys using a new tool called Interactive Model Evaluation and Diagnostics System (IMEDS) developed by the USACE (Devaliere and Hanson, 2009; Hanson et al., 2009). Detailed spectral analysis has only been carried out at a select number of National Data Buoy Center (NDBC) buoys where we have access to the 1D and (if available) 2D spectral records.

There have been numerous validation studies of the WAVEWATCH III^{TM}model that have been carried out over the years (Tolman, 2002a; Hanson et al., 2009; Bidlot et al., 2007). Our motivation for this study was to develop a detailed baseline validation of the multi-grid system that we have setup for NCEP. The study spans a number of years to look for seasonal trends. The availability of new tools such as IMEDS also provide more detailed analysis. Furthermore, though the model has been numerically upgraded, the physics packages in the model have not been changed since they were developed by Tolman and Chalikov (1996) and the last re-tuning of the wave model was done in 2002 (Tolman, 2002a). A 4 year NOPP initiative has recently been approved to upgrade the physics packages in operational third generation wave models. The initiative starts later this year and aims to improve the representation of present source terms as well as develop new source terms for physical processes that are not yet represented in these types of models. Most of the funded work will directly involve WAVEWATCH III^{TM}. In that regard the present study provides the current global skill assessment of **NMWW3**.

2 MODELING SYSTEM

The **NMWW3** system uses an 8 grid mosaic with a global 0.5° grid and multiple higher resolution regional and coastal grids in the areas where the National Weather Service (NWS) has the responsibility to provide forecasts (Fig. 1). Due to computational constraints as well as a lack of need for providing

*MMAB Contribution no. 281
[†]arun.chawla@noaa.gov

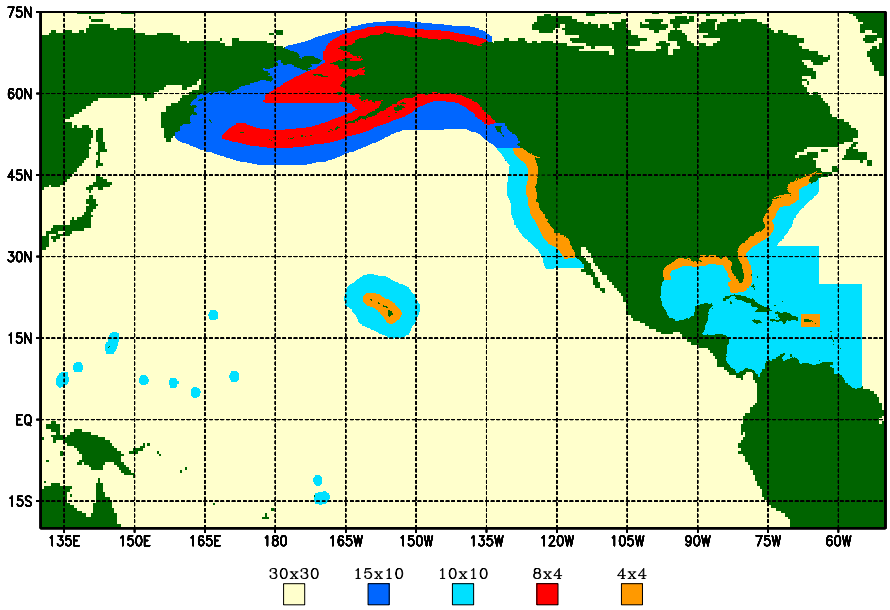

Fig. 1: Grids for NCEP wave modeling system. Grid resolution given in minutes. The global domain (not completely shown here) extends from 77.5°S to 77.5°N and 0° to 359.5°W.

guidance by the NWS, certain bodies of water (e.g. Mediterranean Sea, Hudson Bay, Persian Gulf) have been masked out. The hindcast runs use the same system as the operational forecast runs with the addition of a 9^{th} Arctic Ocean grid (with the same resolution as the global grid) that allows the domain to be extended from 77.5°N to 83°N (this additional grid will be added to the operational system at a yet to be scheduled upgrade later this year).

The model is forced using 10m winds that are obtained from the GFS model. The wind information is extracted from the first sigma layer and converted to 10m winds using a 1D boundary layer model. Wind data is stored on a 0.5° grid and internally interpolated to the individual grid resolutions in **NMWW3**. For the hindcasts we use analysis winds from the Global Data Assimilation System (GDAS) (Kanamitsu, 1989; Derber et al., 1991). Daily sea ice concentration data are generated over a global 1/12° grid using an automated passive microwave analysis (Grumbine, 1996).

3 INTERACTIVE MODEL EVALUATION AND DIAGNOSTICS SYSTEM - IMEDS

IMEDS is an analysis tool that has been developed by the United States Army Corps of Engineers (USACE) for spectral wave models (Hanson et al., 2009). The aim is to have a tool that provides a more detailed spectral evaluation of model performance than the classical comparison of bulk parameters such as significant wave height, but at the same time, still develop quantifiable skill metrics for the model.

IMEDS uses a partitioning algorithm (Hanson, 1996; Hanson and Phillips, 2001) to identify individual peaks (or wave components) in a 2D (or 1D) wave spectrum and classifies them as either wind sea or swell. Fig. 2 shows how a 2D spectrum is partitioned into 3 wave components. The separation between wind sea and swells is done using a directional wave age criteria (Hanson and Phillips, 2001) that involves computing wave age from winds along the wave direction.

Fig. 3 shows the different components of IMEDS. It uses wave buoy data to compute the partition boundaries in a particular spectrum, similar to the one shown in Fig. 2. The same boundaries are then used to denote individual wave components in the model spectra, and spectral attributes (wave height, peak period and direction) for both the model and data are computed. For error analysis the standard error estimates of bias, root mean square error and scatter index are computed for individual component pairs (model and data) on a monthly basis. Error analysis can be done for Temporal Correlations (time paired observations and simulations) or Quantile-Quantile distributions. In this study we

shall limit ourselves to Temporal Correlations. The error metrics are explained in detail in Hanson et al. (2009) and are reproduced here for convenience in analyzing the results.

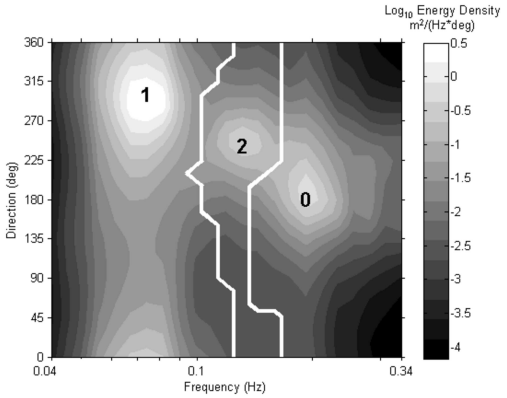

Fig. 2: Wave partitioning of a 2D spectrum in IMEDS. White lines denote the partition boundaries as estimated in IMEDS.(0 → wind wave component; 1 → primary swell; 2 → secondary swell). This is Fig 2 in Hanson et al. (2009)

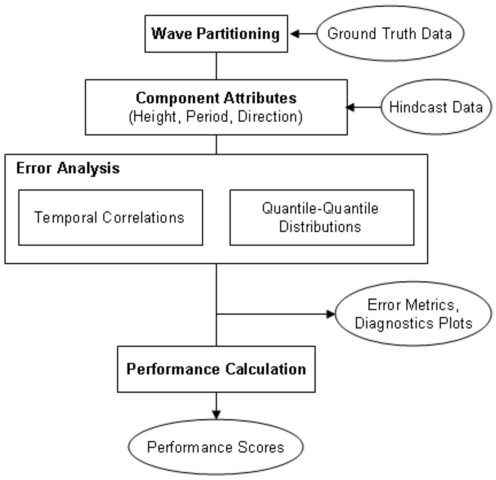

Fig. 3: A schematic view of the different components of IMEDS. This is Fig 1 in Hanson et al. (2009)

The non-directional spectral error metrics are given by

$$b = \frac{1}{n}\sum m - o \tag{1a}$$

$$E_{RMS} = \sqrt{\frac{\sum (m-o)^2}{n}} \tag{1b}$$

$$SI = \frac{\sqrt{\frac{(m-o-b)^2}{n-1}}}{\bar{o}} \tag{1c}$$

where, m and o refer to model and observation parameters (significant wave height H_s or peak period T_p) of individual spectral components respectively, n the number of samples, b is the bias, E_{RMS} the root mean square error and SI the scatter index.

For directional data the angular bias and circular correlation are also computed

$$b_a = \begin{cases} \arctan\left(\frac{S}{C}\right) & \text{for } S>0, C>0, \\ \arctan\left(\frac{S}{C}\right)+\pi & \text{for } C<0, \\ \arctan\left(\frac{S}{C}\right)+2\pi & \text{for } S<0, C<0. \end{cases} \tag{2a}$$

$$cor = \frac{\sum \sin(\theta_o - \bar{\theta}_o)\sin(\theta_m - \bar{\theta}_m)}{\sqrt{\sum[\sin(\theta_o - \bar{\theta}_o)]^2 \sum[\sin(\theta_m - \bar{\theta}_m)]^2}} \tag{2b}$$

where S and C are a measure of the directional differences and are given by

$$S = \sum \sin(\theta_m - \theta_o) \qquad C = \sum \cos(\theta_m - \theta_o)$$

, and θ refers to the average direction for each component.

IMEDS also computes an overall performance score that ranges from 0 (no correlation) to 1 (perfect correlation). To obtain this score it first normalizes all the error estimates (except for *cor* which is already normalized).

$$\begin{aligned} \hat{E}_{RMS} &= \left(1 - \frac{E_{RMS}}{o_{RMS}}\right) \\ \hat{b} &= \left(1 - \frac{|b|}{o_{RMS}}\right) \\ \hat{SI} &= (1 - SI) \\ \hat{b_a} &= \left(1 - \frac{|b_a|}{180}\right) \end{aligned} \tag{3}$$

where o_{RMS} is the root-mean-square of the measurements. The overall performance scores are the averages of the normalized error estimate and are given by

$$\begin{aligned} P_s &= \frac{\hat{E}_{RMS} + \hat{b} + \hat{SI}}{3} \quad \text{(non-directional metrics)} \\ P_s &= \frac{\hat{b_a} + corr}{2} \quad \text{(directional metrics)} \end{aligned} \tag{4}$$

When combining metrics across several months and stations, IMEDS weighs each metric by the sample

size. We shall use this approach in this paper to obtain yearly skill scores for select NDBC buoys in the Atlantic and Pacific to compare the model performance in the two basins.

4 DATA ANALYSIS

Data analysis has been done using 3 different sources of data – altimeter data from the Jason-1 satellite to obtain spatial maps of error estimates, bulk spectral estimates from a global network of buoys to look at detailed temporal patterns at different locations in the world and spectral analysis using IMEDS to estimate which part of the spectrum plays a dominant role in the overall errors of the system.

4.a Altimeter comparisons

For altimeter comparisons we rely on the Jason-1 satellite data to provide estimates of H_s. The altimeter data used is the so called "fast delivery" data which is available in near real time. Since the modeling system went into operations daily files of altimeter and collocated model (for hindcast and several forecast periods) are being generated and archived as part of the operational suite of products. Error metrics have been computed using month long records of this daily archive to ensure global coverage. Calibration and validation of the fast delivery satellite data with buoy measurements was done by Tolman et al. (2006) and as part of this study were confirmed again using the 2008 altimeter data set (figure not shown).

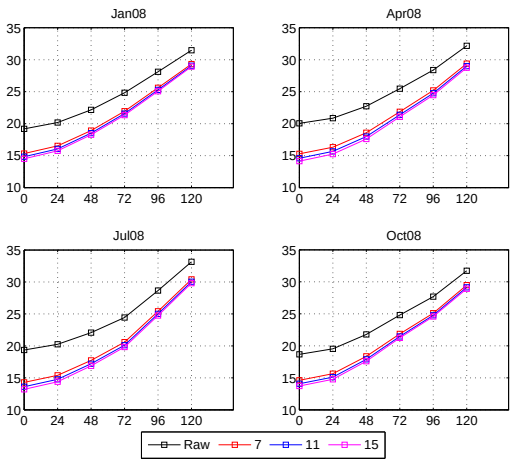

Fig. 4: Scatter Index as a function of forecast hour for four different months. Different lines correspond to different levels of smoothing

The error metrics used here for model analysis have the same definitions as eqn. (1). A de-spiking algorithm is used to remove spikes in the altimeter data. The de-spiking algorithm also accounts for islands that lie along the altimeter track, but are too small to be resolved in the model domain. One of the issues with satellite data is that the data sets are very noisy, which leads to erroneously larger estimates of scatter indices, particularly in periods of low wave heights. To separate the instrument noise from model-data deviations, a running average is used to smooth the altimeter data.

Figure 4 shows the scatter index (SI) computed using raw and averaged altimeter data as a function of the forecast period. The SI for any particular month is computed using the collocated model and data over the entire global domain for that period. Model data at multiple synoptic times of the forecast are collocated with the altimeter data to provide a global skill assessment of **NMWW3**. The error metric does not show any seasonal variability and this will also be seen in the buoy data later in the paper. There is also a significant difference between the raw and the averaged data but not too much difference between the three different levels of averaging. One of the dangers of smoothing data along the altimeter track is that we may mis-represent systems with sharp fronts. We thus want the minimal averaging window that provides accurate error metrics. The SI grows more slowly over the first 48 hours of forecast and faster after that. A scatter index estimate alone is not a good measure of the skill of the forecast (as it does not account for biases and large index estimates may be driven by very small wave heights observations). That said, over the global domain, indices in the range of mid 20's and below, provide valuable guidance information to forecasters. With that in mind, **NMWW3** provides good forecasts out to 96 hours, and anything beyond that should be viewed with a greater degree of uncertainty.

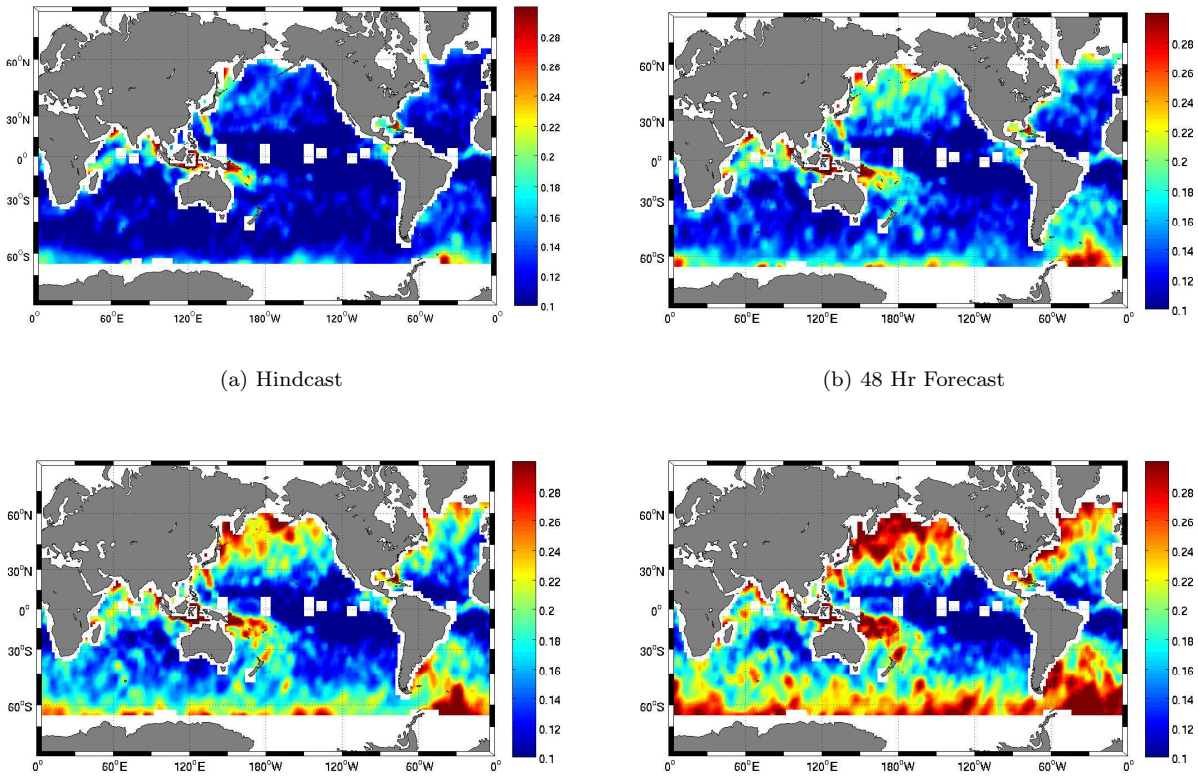

(a) Hindcast

(b) 48 Hr Forecast

(c) 72 Hr Forecast

(d) 96 Hr Forecast

Fig. 5: Scatter Index map of Hs for different periods of the forecast cycle. Map is generated by binning collocated model and altimeter data into $2^\circ \times 2^\circ$ bins. Collocated data from January through March 2008 is used to provide enough points per bin for statistical analysis. A 3-point running average along the longitudes and latitudes is also applied to remove the signature of the tracks

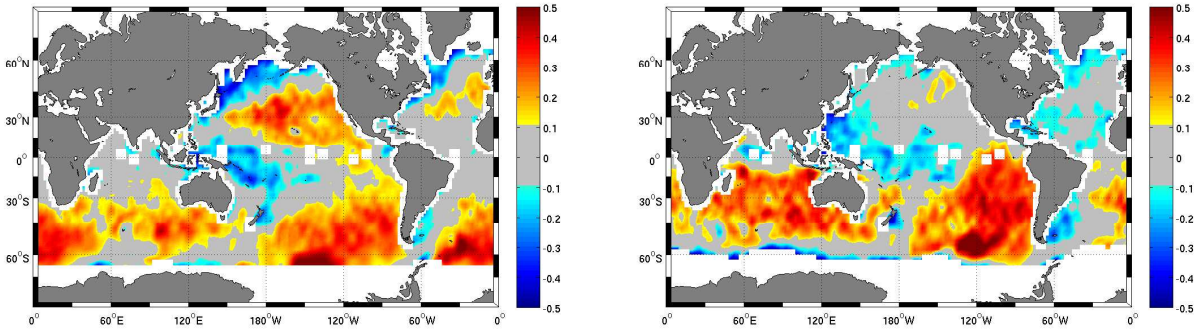

(a) Jan − Mar

(b) Jul − Sep

Fig. 6: Bias maps of Hs hindcast simulations during the winter (a) and summer (b) periods. Bias maps are generated the same way as the SI maps (see caption of Fig 5 for details)

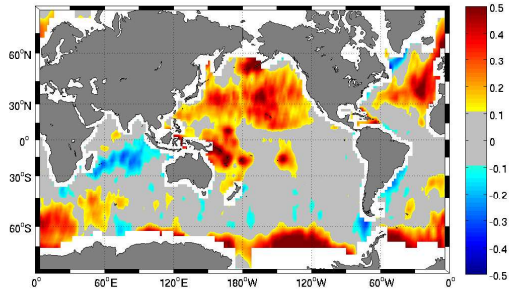

Fig. 7: Bias map of wave hindcasts for the period Jan - Mar 2002. The model used in this data was the older generation **NWW3** model and the satellite data is from the ERS-2 satellite.

Moving from an overall SI measure to a spatial map of indices (Fig. 5) we see that in general the indices are lower at the eastern end of a basin as opposed to the western end (true for both the Pacific and Atlantic basin). This is because winds in general move from west to east, so the western part of the basin is an area of wave generation and dominated by wind waves, which is a more dynamic and localized wave field. Thus even if the model gets the wave growth right, but misses the location, there would be significant error. On the other hand, the eastern end of the basin is more swell dominated, which tend to be much more stable and spread out (in space) in comparison to the wind waves, hence leading to better comparisons between model and data.

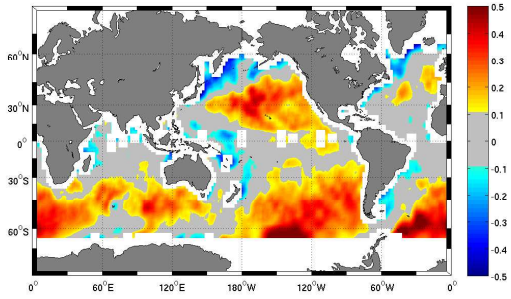

Fig. 8: Bias map of wave hindcasts for the period Jan - Mar 2008 for the **NWW3** model. Satellite data is from Jason-1.

The bias maps (Fig. 6) show a seasonal variability in the Northern Hemisphere that is not seen in the SI plots. During the winter months we see a positive bias in the Pacific basin that extends from the center of the basin all the way to the western coastline of the continental United States. This feature is also seen to a smaller degree in the Atlantic basin. At the same time the western part of the basins show a persistent negative bias. The nature of these biases will be studied in greater detail in the analysis of buoy data later in this section.

The bias maps also show a persistent positive bias over large regions in the Southern Hemisphere. These biases have increased considerably in comparison to the older model (see Fig. 7). The modeling system that was used to generate the data for Fig. 7 was based on WAVEWATCH-III v 2.22 and was a single grid model (referred to as **NWW3**) with a global domain grid resolution of $1.25°\times1°$. For the period corresponding to this figure, the wave model still did not have the island obstruction algorithm of Tolman (2003) implemented, thus leading to the bulls-eye patterns behind major island chains in the bias maps. Accounting for this, we still see a positive bias over large swathes of the Southern Hemisphere in **NMWW3** that was absent in **NWW3**. Even though there have been considerable changes between the two systems, the underlying physics have remained largely unchanged. To confirm that the changes in the bias patterns are not driven by changes to the modeling system, we also plotted the biases for the same period as in Fig. 6 using **NWW3** (Fig. 8). Since the bias patterns for 2008 are similar for the two modeling systems, and distinctly different from the patterns in 2002, the changes are driven by something other than changes to the modeling system. Even though we have used data from two different satellites (ERS-2 and Jason-1) to highlight the recent development of persistent bias in the Southern Hemisphere, these patterns are also confirmed by buoy comparisons (section 4.b).

4.b Buoy Comparisons

To foster a better understanding of operational wave modeling and encourage collaboration, an initial data exchange program was established in the mid 1990s to compare the wave modeling systems at the different operational centers in the world. This program was expanded under the auspices of the Joint Technical Commission for Oceanography and Marine Meteorology (JCOMM) and now includes several centers (Bidlot et al., 2007). As part of that inter-comparison program ECMWF collects and maintains a central archive of buoy data. The archive consists of bulk spectral parameters and includes data from over 250 buoys all over the world. The hourly buoy data have been averaged over a ±2 hr interval centered at the 4 synoptic time cycles (0,6,12 and 18) at which model forecasts are run.

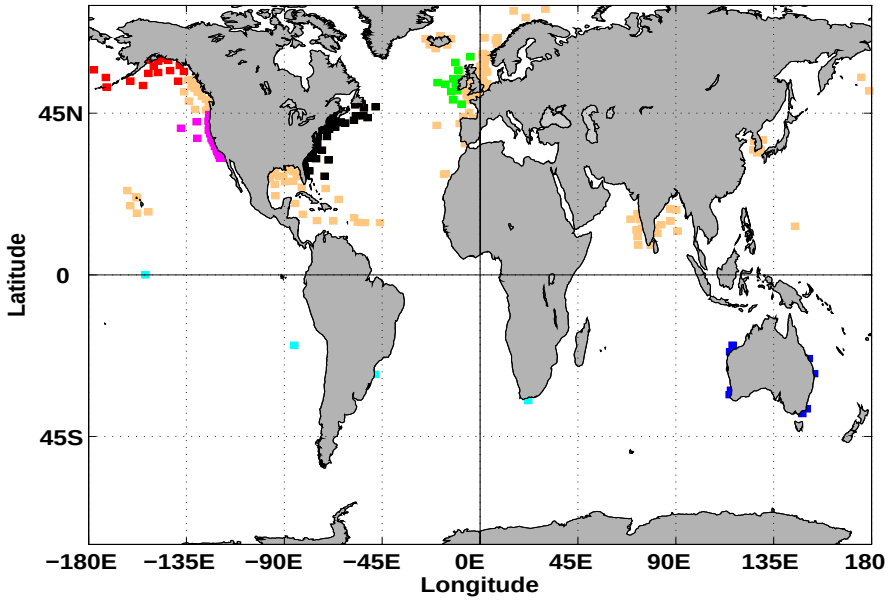

Fig. 9: Location of buoys used in computing error metrics. Buoy data used in the present paper are color coded according to region and error metrics of each region are given in Fig. 10. ('Red' → Alaska;'Magenta' → US West Coast; 'Black' → US East Coast; 'Green' → Europe; 'Cyan' → Southern Hemisphere; 'Blue' → Australia)

Processing and quality control of these data are done at ECMWF. We have used this data set to compare with the model hindcasts.

Fig. 9 shows the locations of the different buoys. The buoys have been grouped by region, and only those regions for which the results are shown in this paper are identified by color. The error metrics for the different regions as a function of time can be seen in Fig. 10. The seasonal biases that was alluded to in section 4.a can be clearly seen in the time series plots. The buoys along the US East Coast and in the Alaskan waters show a negative bias while the buoys along the US West Coast show a positive bias pattern. These are very consistent with the bias maps in Fig. 6. Just like in the eastern part of the Pacific basin, a positive bias pattern is also seen in the eastern part of the Atlantic basin (European buoys) though the magnitudes (with the exception of one year) are generally weaker. We can also see the development of the same persistent positive bias in the buoys of the Southern Hemisphere. The data indicates that these patterns have started to grow since 2006. SI measures do not show much of the seasonal trend seen in the bias plots and tend to be fairly low everywhere. Like the altimeter data, buoy data also shows the tendency for the indices to be larger in buoys that lie in areas dominated by wind seas (such as the US East Coast) as opposed to swells (US West Coast).

4.c IMEDS Comparison

IMEDS has been used to study the bias patterns in more detail. IMEDS analysis has been limited to the National Data Buoy Center (NDBC) buoys, as we have access to detailed spectral records from these buoys. Since the bulk spectral parameters show such distinct patterns along Alaska, US West Coast and US East Coast, buoys from these three regions have been selected for analysis (Fig. 11).

While IMEDS uses a directional wave-age criteria to separate locally generated wind seas from swells. The individual swells are further classified as young or mature swells based on the peak frequencies in the data being greater or less than 0.09Hz, respectively (Hanson et al., 2009). Error metrics are then computed for the 3 different classes of wave fields.

IMEDS analysis was done using the 2007 and 2008 hindcast data sets. Table 1 shows the skill set scores (obtained from eqn. 4) of the individual components for the different regions. The scores generally show that the model performs better in predicting the peak period T_p than the significant wave height H_s. Also the scores for the Atlantic region were the worst and the Pacific region the best with the Alaskan re-

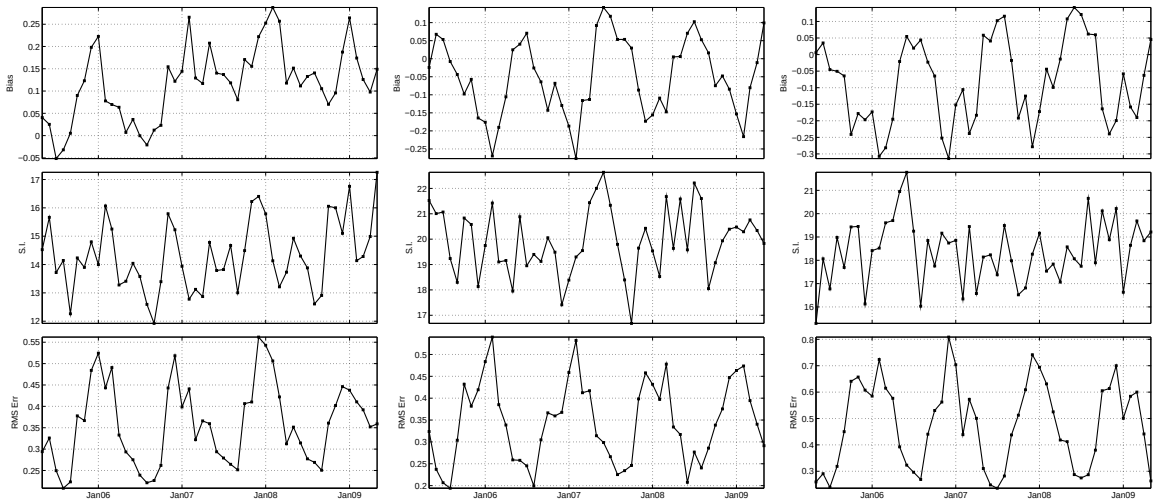

(a) U.S. West Coast (b) U.S. East Coast (c) Alaska

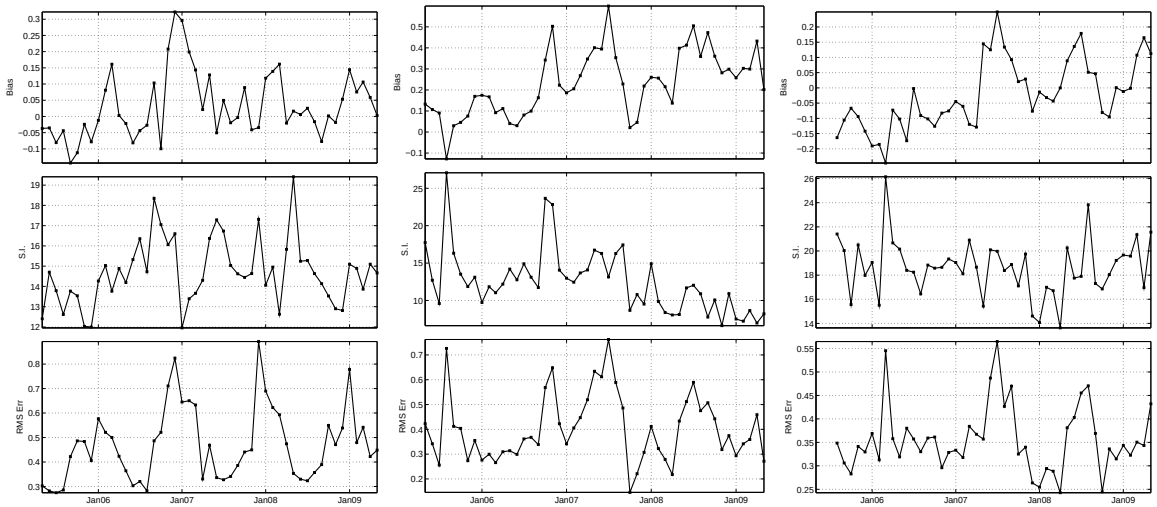

(d) Europe (e) Southern Hemisphere (f) Australia

Fig. 10: Error metrics of wave hindcast Hs at buoys for the hindcast period of May 2005 through May 2009. Both bias and RMS error are in m. Map showing the buoy locations for each region is given in Fig 9.

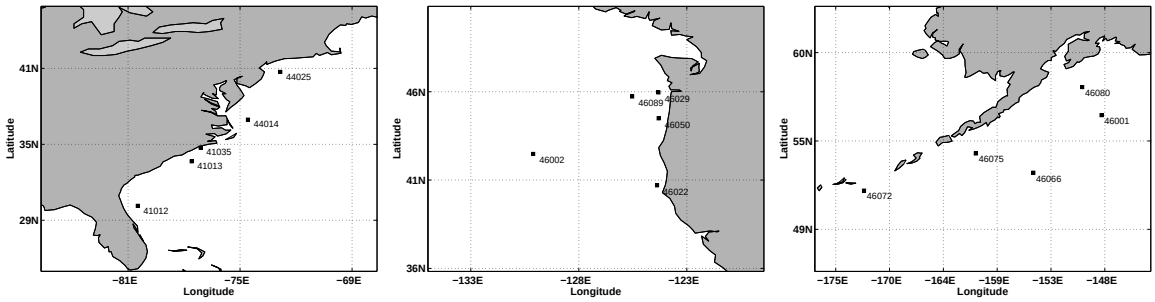

(a) Atlantic (b) Pacific (c) Alaska

Fig. 11: NDBC Buoys used in IMEDS analysis. Buoys are identified by their unique IDs provided by NDBC

Component		Atlantic			Pacific			Alaska		
		H_s	T_p	θ	H_s	T_p	θ	H_s	T_p	θ
Wind Sea	2007	0.83	0.85	0.96	0.89	0.85	0.95	0.88	0.86	-
	2008	0.85	0.84	0.94	0.9	0.86	0.94	0.87	0.86	-
Young swell	2007	0.82	0.92	0.83	0.83	0.9	0.92	0.85	0.89	-
	2008	0.83	0.91	0.92	0.85	0.91	0.92	0.85	0.89	-
Mature swell	2007	0.75	0.87	0.8	0.81	0.95	0.89	0.84	0.93	-
	2008	0.75	0.88	0.79	0.8	0.94	0.87	0.79	0.93	-
Full Spectrum	2007	0.84	0.84	0.88	0.89	0.85	0.8	0.88	0.83	-
	2008	0.85	0.83	0.84	0.89	0.86	0.82	0.87	0.83	-

Table 1: IMEDS Performance Scores (by region) for 2007 & 2008 buoy data

gion being in between. This is similar to what we observed from the altimeter and bulk spectral parameter comparisons at the buoys. The scores across the two years are fairly similar and thus, for brevity only the plots from the 2008 data sets are shown here.

Results from the IMEDS analysis for the different regions is shown in Figs. 12 − 14. Apart from plots of the error estimates for the individual components, scatter plots at select stations have also been shown. The scatter plots at any location show the distribution of the different wave components (and their magnitude) at that location over the month.

The overall bias in the Atlantic buoys (Fig. 12) shows a seasonal pattern with greater negative bias values in the winter months and lower values during the summer months. The exception being buoy 41035 which shows a consistent negative bias. This may be because the buoy is in fairly shallow water (depth 10m) and the depth may not be well represented in our grids. Also, being very close to the coast, the wind is probably not very well represented either (wind data is linearly interpolated from a 0.5° grid, and very close to the coastline, down scaling effects that accurately account for land-sea transitions can become very important). The buoys are predominantly dominated by wind waves and young swells, with very few instances of mature swells. In general, the different components show a negative bias most of the time, except for buoy 41012, which shows a slight positive bias in the young swells (this was observed in the 2007 data too). It should be pointed out that the separation between young and mature swells in IMEDS is based on a peak frequency cutoff that was seen to be generally true for the Pacific basin (Hanson et al., 2009), and may not hold true for the Atlantic basin.

The Pacific buoys (Fig. 13) on the other hand show a positive bias pattern. The wind seas show the same negative bias that is seen in the Atlantic buoy data, but the swells have a positive bias pattern. In particular the mature swells show a greater bias during the winter months as opposed to the summer months. And, as can be seen from the scatter plots, there are a lot more swell systems at these buoys, leading to an overall seasonal positive bias pattern.

The Alaska buoys (Fig. 14) lie somewhere in between the Atlantic and Pacific buoys in their error characteristics. While the wind sea components show the negative bias patterns during the winter months just like the Atlantic and Pacific buoy data the swells show a range of bias patterns that range from positive to negative. Scatter plots indicate that the buoys in this area have a mix of wind wave and swell seas.

5 DISCUSSION

A global modeling system based on the WAVEWATCH III^{TM}model and GFS winds has been analyzed using a multi-year hindcast database (as well as archived forecasts). The basic features that we have found are

- Scatter indices well below 25, with much lower values in the swell dominated eastern parts of the ocean basins.
- Seasonal patterns to bias, specially in the Northern Hemisphere. A negative seasonal bias along the wind wave dominated western parts of the ocean basins and a positive seasonal bias along the swell dominated eastern parts.
- The recent development of a persistent positive bias in the Southern Hemisphere.

One possible reason for persistent increased biases in the Southern Hemisphere could be that the representation of the winds in this region by the GFS model has changed since the last time that the wave model was tuned (2000-2001). Fig. 15 shows the wind statistics (from the GFS model) over water in both the Southern and Northern Hemisphere. Since 2005, we can see a clear upward shift in the higher wind speeds, leading to a significant change in the 99^{th} percentile curves, with minimal impact on the average wind speeds. And since wave growth is a non-linear process, this manifests as a positive bias in the wave model. Comparing with the Southern Hemisphere buoy statistics in Fig. 10, we can see that the increased bias in this region coincides with the changes in the GFS winds. The winds in the Northern Hemisphere over the same period did not show any significant changes. It remains to be seen if a new database of high resolution re-analysis winds (currently under development at NCEP) will show the same results.

The bias patterns that we see in the Pacific buoys are very similar to the patterns seen by Hanson et al. (2009) in their hindcast simulations. Comparing with the bias patterns at other buoys in the Northern Hemisphere it seems that the wave model

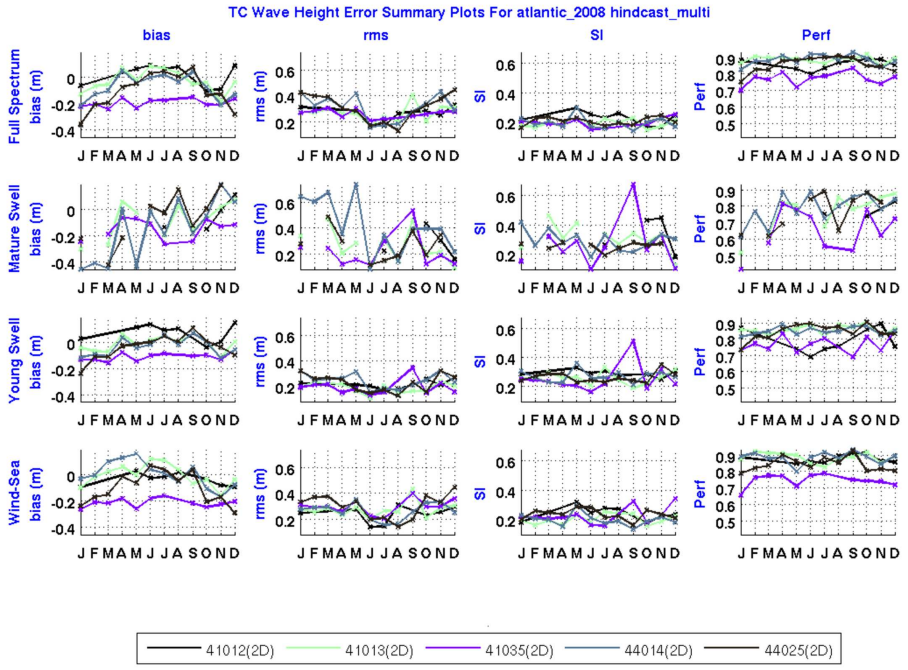

(a) Error Summary

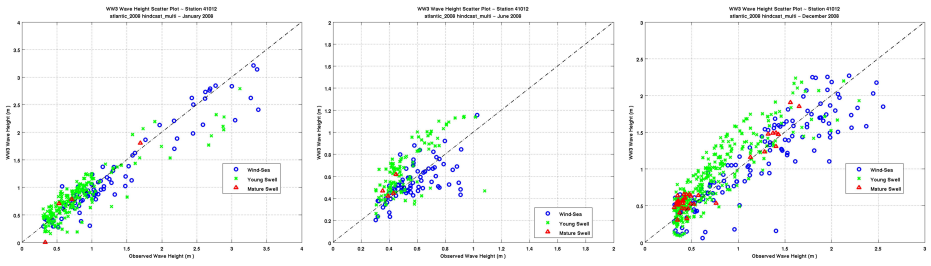

(b) 41012 – January (c) 41012 – June (d) 41012 – December

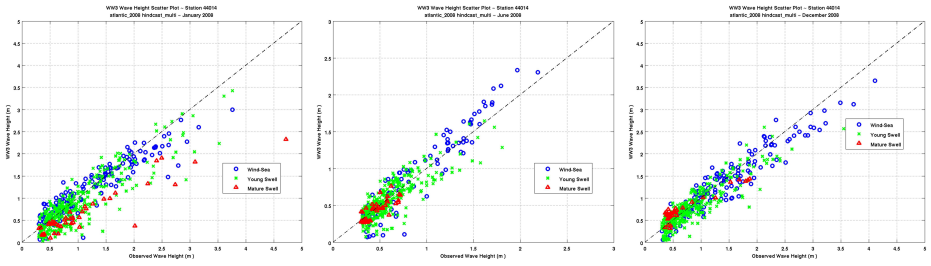

(e) 44014 – January (f) 44014 – June (g) 44014 – December

Fig. 12: IMEDS analysis of H_s data for 2008 Atlantic bouys. Panel (a) shows the error summaries for the different buoys. Panels (b) - (g) show the scatter plots of individual components for select buoys at select periods of time. 'Blue' $\circ \rightarrow$ wind waves; 'Green' $\star \rightarrow$ Young swells; 'Red' $\triangle \rightarrow$ Mature swell. All the figures have been generated by the IMEDS package

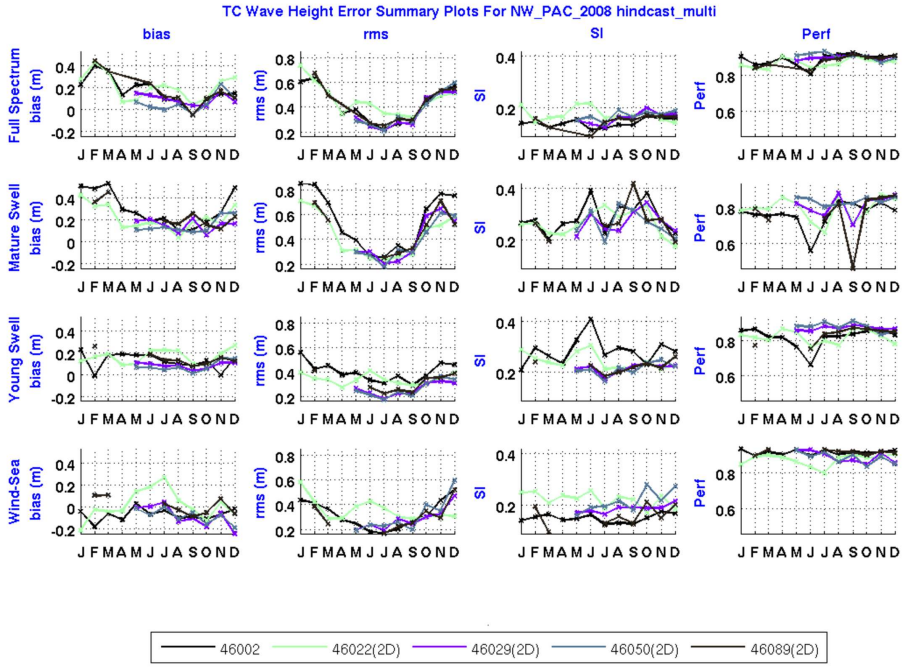

(a) Error Summary

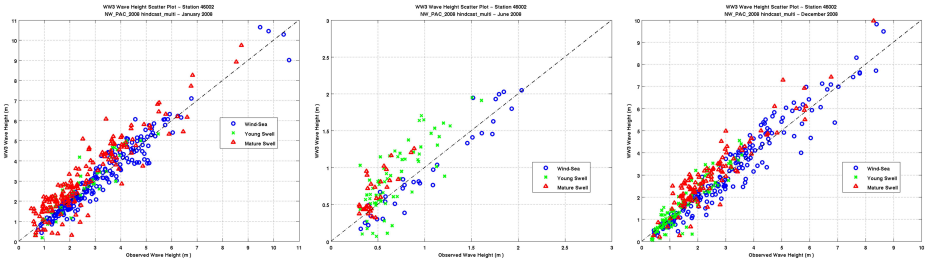

(b) 46002 – January (c) 46002 – June (d) 46002 – December

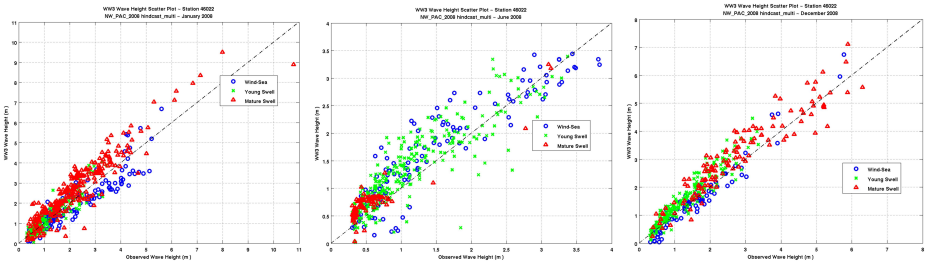

(e) 46022 – January (f) 46022 – June (g) 46022 – December

Fig. 13: IMEDS analysis of H_s data for 2008 Pacific bouys. See caption of Fig. 12 for detailed information on individual panels.

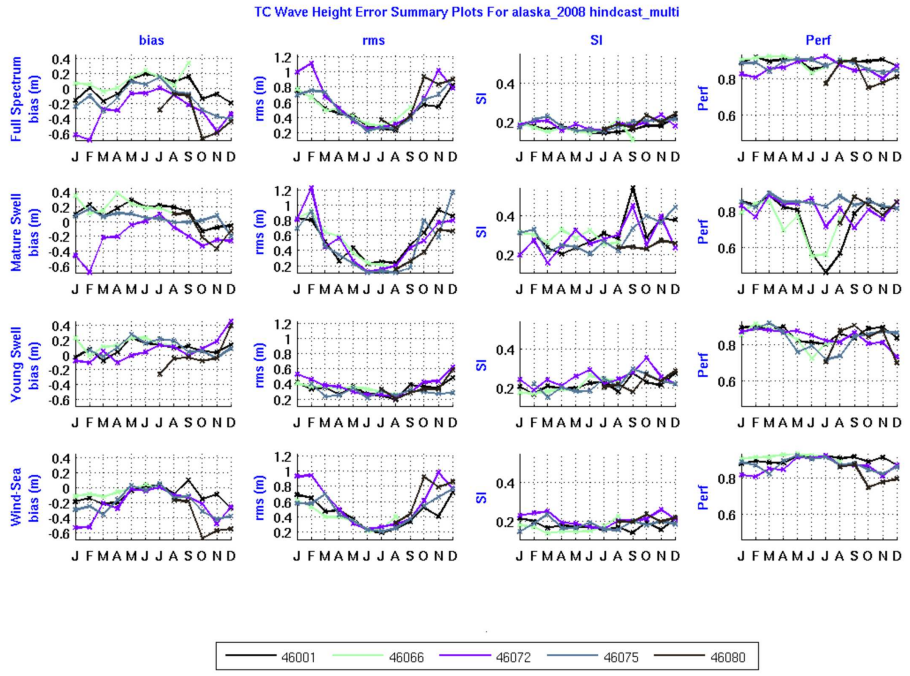

(a) Error Summary

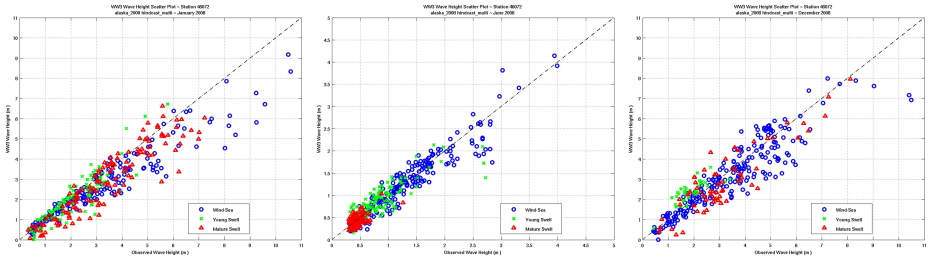

(b) 46072 – January (c) 46072 – June (d) 46072 – December

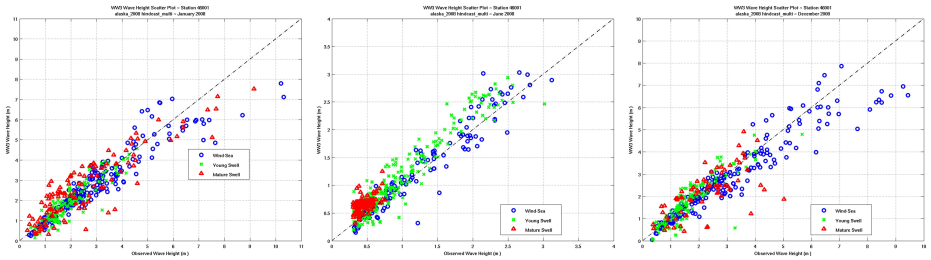

(e) 46001 – January (f) 46001 – June (g) 46001 – December

Fig. 14: IMEDS analysis of H_s data for 2008 Alaska bouys. See caption of Fig. 12 for detailed information on individual panels.

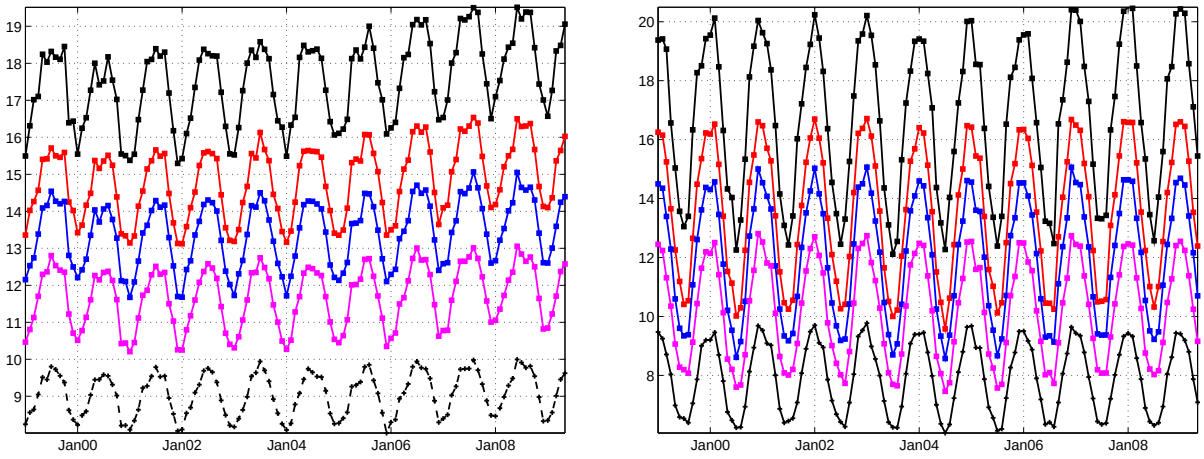

(a) Southern Hemisphere

(b) Northern Hemisphere

Fig. 15: Wind speed statistics for the 10m winds from the GFS model. Statistics have been computed separately for the Southern Hemisphere (defined by 60°S to 25°S) and Northern Hemisphere (defined by 25°N to 60°N). All land points have been excluded. The y axis refers to wind speed in (m/s). The dashed line is the average speed, and the solid lines refer to the different percentiles ('Black' → 99 percentile; 'Red' → 95 percentile; 'Blue' → 90 percentile; 'Magenta' → 80 percentile)

is slightly under predicting the growth in the wind seas, which leads to an initial under prediction of the swells. However, once the energy is transferred to the swells, it does not dissipate the energy fast enough. The patterns of swell bias (generally negative in the Atlantic buoys, positive in the Pacific buoys and mixed in the Alaska buoys) seem to indicate that the bias is related to the origin of the swell, however, more analysis of swell dissipation in the model needs to be done before such a conclusion can be decisively reached. Swell dissipation is as yet a poorly understood topic, and while such a term exists in WAVEWATCH III$^{\text{TM}}$, it is primarily a tuning parameter to reduce overall error (Tolman, 2002c; Hanson et al., 2009). Recently Ardhuin et al. (2009) have tried to decipher the nature of this dissipation parameter using SAR data sets and have concluded that the dissipation is non-linear and related to wave steepness. As has been pointed out, the separation between mature and young swells in IMEDS is currently based on a frequency cut-off that was seen to hold in general for the Pacific basin. A more accurate approach would be to identify swells by their area of origin so that bias patterns can be mapped against propagation distance. This would allow us to see if inaccurate swell dissipation is the main cause of bias errors in the wave model, or it is related to other processes (e.g. non-linear energy transfer, wave - surface drag interactions etc.). It is possible to identify and follow individual wave system in IMEDS and this topic will be explored further.

WAVEWATCH III$^{\text{TM}}$has two tunable parameters (for wave growth and swell dissipation), that can be used to reduce overall errors in the model simulations. Model - data comparisons indicate that it may be worthwhile to revisit these parameters, specially with regard to the changing wind fields in the GFS model. However, we are also in the beginning stages of an extensive NOPP study to develop new physics packages for the third generation wave models. The focus of the NOPP study includes new wave growth and dissipation terms, more advanced nonlinear algorithms, as well as swell dissipation terms, among others. In lieu of this, wave parameter tuning may be delayed till the new packages are in place.

References

Ardhuin, F., B. Chapron and F. Collard, 2009: Observation of swell dissipation across oceans. *Gephys. Res. Lett.*, **36**(L06607).

Bidlot, J. R., J. G. Li, P. Wittmann, M. Faucher, H. S. Chen, J. M. Lefevre, T. Bruns, D. Greenslade, F. Ardhuin, N. Kohno, S. Park and M. Gomez, 2007: Inter-comparison of operational

wave forecasting systems. in *10th International workshop on wave hindcasting and forecasting*, Oahu, Hawaii.

Chawla, A., D. Cao, V. Gerald, T. Spindler and H. Tolman, 2007: Operational implementation of a multi-grid wave forecasting system. in *10th International workshop on wave hindcasting and forecasting*, p. pp 12, Oahu, Hawaii.

Derber, J. C., D. F. Parrish and S. J. Lord, 1991: The new global operational analysis system at the National Meteorological Center. *Weather and Forecasting*, **6**, 538–547.

Devaliere, E.-M. and J. Hanson, 2009: *IMEDS Interactive Model Evaluation and Diagnostics System V2.6 Users Guide*. US Army Corps of Engineers, Field Research Facility, Duck, NC.

Grumbine, R. W., 1996: Automated passive microwave sea ice concentration analysis. Technical note 120, NCEP/NOAA/NWS, National Center for Environmental Prediction, Washington DC.

Hanson, J. L., 1996: *Wind sea growth and swell evolution in the Gulf of Alaska*. Ph.D. thesis, Johns Hopkins University.

Hanson, J. L. and O. M. Phillips, 2001: Automated analysis of ocean surface directional wave spectra. *J. Atmos. Oceanic Technol.*, **18**, 277 – 293.

Hanson, J. L., B. A. Tracy, H. L. Tolman and R. D. Scott, 2009: Pacific hindcast performance of three numerical wave models. *Journal of Atmospheric and Oceanic Technology*, **26**, 1614 – 1633.

Kanamitsu, M., 1989: Description of the NMC global data assimilation and forecast system. *Weather and Forecasting*, **4**, 335–342.

Moorthi, S., H.-L. Pan and P. Caplan, 2001: Changes to the 2001 ncep Operational MRF/AVN Global Analysis/Forecast System. Technical Procedures Bulletin 484, NWS/NCEP.

Tolman, H. L., 2002a: Testing of WAVEWATCH III version 2.22 in NCEP's NWW3 ocean wave model suite. Technical note 214, NCEP/NOAA/NWS, National Center for Environmental Prediction, Washington DC.

Tolman, H. L., 2002b: User manual and system documentation of WAVEWATCH III version 2.22. Technical note 222, NCEP/NOAA/NWS, National Center for Environmental Prediction, Washington DC.

Tolman, H. L., 2002c: Validation of WAVEWATCH III version 1.15 for a global domain. Technical note 213, NCEP/NOAA/NWS, National Center for Environmental Prediction, Washington DC.

Tolman, H. L., 2003: Treatment of unresolved islands and ice in wind wave models. *Ocean Modelling*, **5**, 219 – 231.

Tolman, H. L., 2008: A mosaic approach to wind wave modeling. *Ocean Modelling*, **25**, 35–47.

Tolman, H. L., D. Cao and V. M. Gerald, 2006: Altimeter data for use in wave models at ncep. Tech. Rep. 252, NCEP/NOAA/NWS, National Center for Environmental Prediction, Wasjington DC.

Tolman, H. L. and D. Chalikov, 1996: Source terms in a thrid generation wind wave model. *Journal of Physical Oceanography*, **26**, 2497–2518.